Bull Mater Sci (2020) 43:293
https://doi.org/10.1007/s12034-020-02258-5

Manifestation of descent symmetry phenomena in tetrahedral structure of M_4^{2+} (M = P, As, Sb) analogues

ALI REZA ILKHANI[1,2,*] and WILLIAN HERMOSO[3]

[1]Department of Chemistry, Yazd Branch, Islamic Azad University, Yazd, Iran
[2]Department of Chemistry, University of Alberta, Edmonton, AB T6G 2G2, Canada
[3]Department of Chemistry, Institute of Environmental, Chemical and Pharmaceutical Sciences, Federal University of Sao Paulo, Sao Paulo, Brazil
*Author for correspondence (ilkhaniali@iauyazd.ac.ir)

MS received 13 April 2020; accepted 22 June 2020

Abstract. Manifestation of descent symmetry phenomena induced by pseudo Jahn–Teller interactions is reported for the P_4 dicationic tetrahedral structure and its As_4 and Sb_4 analogues. The symmetry descent phenomena in the dicationic tetrahedral structure for the series is caused by the pseudo Jahn–Teller effect (PJTE) where the unstable (high T_d symmetry) configuration distorts to the equilibrium geometry with a lower, C_2 symmetry. State averaging six low-lying electronic states *via* CASSCF(8,8)/cc-pVTZ–(PP) computations determined the adiabatic potential energy surfaces along the distorting normal coordinate. The $(E_{(I)} + A_1 + E_{(II)}) \otimes e$ for the M_4^{2+} (M = P, As, Sb) series has been formulated accordingly. Subsequently, the coupling constants were estimated by fitting energies obtained from the PJTE equations. Moreover, to understand how removing or adding electrons affects the PJTE in the M_4^{2+} series, electronic configurations were analysed for $M_4^{(0,2+,4+)}$ analogues in which the $M_4^{(0,4+)}$ are stable in their tetrahedral structure.

Keywords. Symmetry descent phenomena; pseudo Jahn–Teller effect; *Ab initio* calculations; ground-excited states interactions.

1. Introduction

The tetrahedral (TH) configuration is a well-known structure constructed by four atoms as the apexes of a triangular pyramid. White phosphorus (P_4) is the most famous stable phosphorus allotrope and it is a popular example of TH tetra-atomic structure. Due to the inoccupation of *d* and *f* atomic orbitals in nitrogen, it possesses drastically different properties with the other elements within Group 15. Thus, nitrogen as the N_4 allotrope does not form a TH structure under current experimental environments. Evidenced by the appearance that yellow arsenic (As_4) and Sb_4 in the TH structure display similar properties to P_4 analogues in the group. The P_4 equilibrium structure was compared with the difference in size of the valence orbital radii and reported by Kutzelnigg [1]. Although the valence orbitals in the nitrogen TH structure have a similar radius with P_4, the nitrogen TH equilibrium configuration is unstable due to the repulsion between atomic orbitals on each N atom is much larger than that for P_4 [2]. The stability of P_4 in a TH structure has been investigated theoretically *via* a dimerization reaction of the P_2 to P_4 allotrope [3] and Schmidt and Gordon [4] has computed phosphorus in linear, TH and cubic forms to compare the stability in the respective configurations. The thermochemical properties and photolytic decomposition pathway from P_2 to P_4 with a TH structure have also been accurately calculated [5,6]. Recently, the C_{2v} thermal decomposition pathway of the TH was investigated by Oakley *et al* [7]. Additionally, the TH structural instability of P_4 in high temperature has been traced experimentally [8] and the first two bands of the P_4 photoelectron spectrum with TH structure were experimentally reported by Wang *et al* [9,10]. This instability is reminiscent of the $E \otimes e$ Jahn–Teller effect (JTE), which is the most well-studied JT problem and a wide range of the literature has documented the exploration of different aspects of it [11–14]. Here, the particularly strong $^2T_2 \otimes (t_2 + e)$ JTE observed belongs to TH structure P_4^+ cation [15].

Since the pseudo Jahn–Teller effect (PJTE) theory is the only source of spontaneous symmetry breaking and symmetry descent phenomena (SDP) in compounds with non-degenerate states and it also explains the origin of the structural instability in polyatomic systems [16], the PJTE has been employed to explain the reason for non-planarity in several unstable two dimensional hetero-cyclic compounds [17–30]. Due to the unique features and specific physical and chemical properties of two-dimensional (2D) materials, such as graphene, the application of the PJTE was an important approach demonstrating the origin of puckering in sheets and explored the reason for non-planarity in

Published online: 12 November 2020

quasi-2D systems with similar expected properties [31–35]. Moreover, manipulation of the puckered cyclic structure by coordinating cationic and anionic forms of atoms and rings can adjust the energy interval between states that are involved in the PJTE. Consequently, the effect is either suppressed, or its intensity decreased [36–39]. Environmental and cooperativity effects in crystalline phases could also provide an essential role to quench the triggers for PJT distortion in 2D-systems [40]. According to new applications of the TH structure in the field of drug delivery [41], investigating the pyramidal tetrahedral structure and the factors that may affect the TH structure is necessary for researchers working in the field of drug delivery.

2. Computational methods

Geometry optimization and following frequency calculations for the ground state of the TH with T_d symmetry and distorted (C_2) configurations of the M_4^{2+} (M = P, As, Sb) analogues were performed at the DFT (B3LYP) level of theory [42]. Subsequently, energy levels of low-lying excited electronic states were state-averaged by the state average–complete active space self-consistent field (SA–CASSCF) wave-function method [43–45] to characterize the adiabatic potential energy surfaces (APESs) along the *e* distortion normal coordinate. For the P_4^{2+} and As_4^{2+} analogues in all calculations, a triple-ζ basis set, cc–pVTZ [46–48], was employed. According to basis set limitations for Sb atom, the pseudopotential cc–pVTZ–PP basis set [49–51] was instead used in the Sb_4^{2+} analogue calculations. Due to the M_4^{2+} analogue's electronic configurations, the (8,8) active space, which is composed number of electrons (8) in active orbitals (8), was selected on account of rationalizing molecular orbital properties in CASSCF computation for the M_4^{2+} series. To maintain a consistent active space in the TH structure for all $M_4^{(0,2+,4+)}$ series, the (10,8) and (6,8) active spaces which add and remove pair of electrons in the highest occupied molecular orbital (HOMO) has been used for the M_4 and M_4^{4+} series, respectively. All calculations were carried out using the MOLPRO 2015 quantum-chemistry program packages [52].

3. Results and discussion

3.1 *Tetrahedral and distorted M_4^{2+} analogues*

The frequency calculations demonstrate that the TH configuration of M_4^{2+} (M = P, As, Sb) analogues have an imaginary frequency possessing *e* symmetry revealing instability in the TH structure. Indeed, the TH in the considered series is not at a minimum and the transformation to the stable C_2 lower-symmetry structure is realized by a *e*-type nuclear distortion. The SDP occurrence in the M_4^{2+} analogues are demonstrated in figure 1 and atoms in different positions are displayed by numbers. The atomic displacements from X or Y axis induced by the distortion are shown by red line.

For the TH (T_d-symmetry) and distorted (C_2-symmetry) configurations of the M_4^{2+} (M = P, As, Sb) analogues, imaginary frequencies correspond to the instability (in cm^{-1}), dipole moment (in 10^{-5} Debye) and calculated geometrical parameters in the form of bond lengths (in Å), angles and dihedral angles (in degrees), respectively. These values are presented in table 1 for both TH configuration and distorted C_2 equilibrium structure.

According to the magnitude of the imaginary frequency in the TH configuration in table 1, instability in the considered analogues corresponds to the size of the atoms. The TH configuration is more distorted in P_4 than other analogues in transferring to its C_2 equilibrium structure with strained triangular rings. In other words, the TH configuration for P_4^{2+} is the most unstable analogue and the instability decreases from P_4^{2+} to Sb_4^{2+}.

Comparing geometrical parameters, the analogues under consideration display changes in all parameters. Some include the 1–4 and 2–3 bonds that undergo a $\sim$14–16% stretch and that the 1–3–4 and 2–4–3 angles increase by $\sim 25-29\%$ from the TH configuration to the distorted equilibrium structure. Furthermore, 4–3–2–1 and 3–4–1–2 dihedral angles raise by 3.4, 2.3 and 1.3 degrees from T_d to C_2 symmetry in the respective P_4^{2+}, As_4^{2+} and Sb_4^{2+} analogues. Additionally, comparing the dipole moment of the dication analogues shows an increase from P_4^{2+} to Sb_4^{2+} in both TH and distorted configurations. Consequently, the polarity of the distorted (C_2 symmetry) structure increases when compared to the TH configuration.

3.2 *Adiabatic potential energy surfaces*

Regarding the transformation to the stable C_2 lower-symmetry structure, the imaginary frequency possessing *e* symmetry in M_4^{2+} analogues and group theory rules, mixing the E ground state with the negative curvature ($E_{(I)}$) with one or more A_1 excited states is the reason of the SDP in the series. Thus, a kind of the $(E_{(I)} + A_1 + \cdots) \otimes e$ problem should be formulated and applied for explaining the origin of the PJTE and determination of their corresponding coupling.

To illustrate the mixed A_1 neighbouring excited states in the PJTE problem, the degenerate E ground and relevant low-lying excited states of the M_4^{2+} analogues were presented as adiabatic potential energy surface (APES) cross-sections of the energy states around the Q_e instability direction in figure 2.

Observing a negative curvature in the $E_{(I)}$ ground state proves that the instability exists along with the possibility of distorting in the TH configuration for all the M_4^{2+} (M = P, As, Sb) analogues. Meanwhile, a positive curvature of the A_1 excited state devises the PJTE $(E_{(I)} + A_1) \otimes e$ problem which was predicted before by the group theory rules. However, any

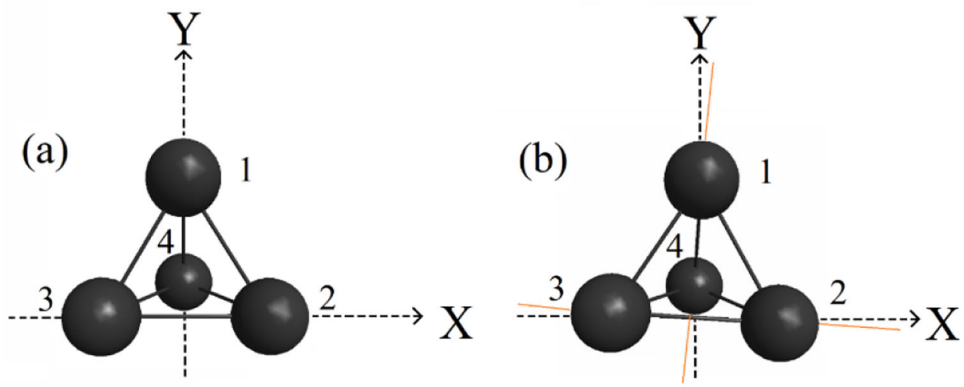

Figure 1. The symmetry descent phenomena occur in M_4^{2+} (M = P, As, Sb) analogues from (**a**) the unstable tetrahedral T_d configuration to (**b**) a stable distorted C_2 structure.

Table 1. Geometry parameters, imaginary frequencies, normal modes and dipole moments of M_4^{2+} (M = P, As, Sb) analogues in unstable tetrahedral configurations (T_d symmetry) and equilibrium structures with C_2 lower symmetry along Q_e deformation normal coordinate.

		Analogues					
		P_4^{2+}		As_4^{2+}		Sb_4^{2+}	
Geometry parameters		Tetrahedral (T_d)	Equilibrium (C_2)	Tetrahedral (T_d)	Equilibrium (C_2)	Tetrahedral (T_d)	Equilibrium (C_2)
Bond length (Å)	1–2	2.321	2.169	2.570	2.403	2.975	2.798
	3–4		2.170		2.403		2.798
	1–4		2.704		2.971		3.412
	2–3						
	1–3		2.171		2.404		2.799
	2–4						
Angle (deg.)	1–2–3	60.00	51.45	60.00	51.83	60.00	52.42
	2–1–4						
	1–2–4		77.09		76.34		75.16
	2–1–3						
	1–3–2		51.46		51.84		52.43
	1–4–2						
	1–3–4		77.09		76.34		75.16
	2–4–3						
	1–4–3		51.45		51.83		52.43
	2–3–4						
	3–1–4		51.46		51.84		52.42
	3–2–4						
Dihedral angle (deg.)	1–3–4–2	70.53	70.39	70.53	70.45	70.53	70.51
	3–1–2–4						
	2–3–1–4		67.24		68.33		69.23
	1–4–2–3						
	4–3–2–1		73.88		72.79		71.84
	3–4–1–2						
Imaginary frequency (cm^{-1})		2624.6	—	1765.0	—	1165.4	—
Normal modes in Cartesian X and Y		±0.0898	—	±0.0578	—	±0.0453	—
Dipole moment × 10^{-5} (Debye)		2.61	6.36	5.18	9.21	9.16	11.2

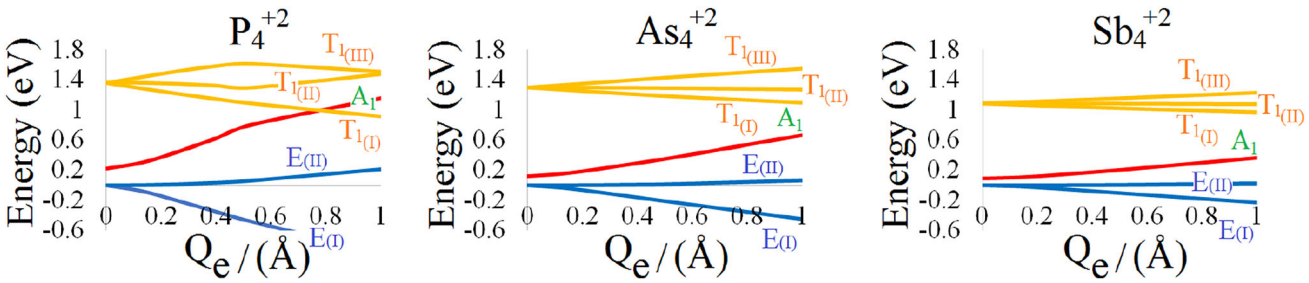

Figure 2. The adiabatic potential energy surface for the M_4^{2+} (M = P, As, Sb) analogues in the Q_e instability puckering direction (Note I, II and III subscripts denote the first, second and third states in the same symmetry, respectively).

low-lying states with E and A_1 symmetries should also contribute to the problem and modify the $(E_{(I)} + A_1 + E_{(II)}) \otimes e$ PJTE problem (see figure 2). Moreover, the difference between the T_1 symmetry and the C_2 distortion structures' effective symmetries (E or A_1) shows that the triply degenerate T_1 ($T_{1(I)}$, $T_{1(II)}$, $T_{1(III)}$) excited states do not emerge in the $(E_{(I)} + A_1 + E_{(II)}) \otimes e$ PJTE problem in the considered M_4^{2+} analogues. In other words, the coupling in the above problem only emerges between the $E_{(I)}$, $E_{(II)}$ degenerate ground states with the low lying A_1 excited states along *e* vibrational mode.

3.3 *Electronic configuration in $M_4^{(2+,0,4+)}$*

Electronic calculations were computed for the doubly degenerate $E_{(I)}$ and $E_{(II)}$ ground state and A_1 and triply degenerate $T_{1(I)}$, $T_{1(II)}$, $T_{1(III)}$, low-lying excited states related to $M_4^{(2+,0,4+)}$ analogues in TH configuration. The main electronic configurations and their weight coefficients for all mentioned states are given in table 2.

From table 2, we can see that the highest weight coefficient in the E degenerate ground state belongs to the ($a_1^2\, e_{(II)}^2\, t_{1(I)}^2\, t_{1(II)}^2$, $a_1^2\, e_{(II)}^2\, t_{1(I)}^2\, t_{1(II)}^2\, e_{(I)}^2$, and $a_1^2\, t_{1(I)}^2\, t_{1(II)}^2$) electronic configurations for the $E_{(II)}$, $E_{(I)}$ states and A_1 excited state, as well as ($a_1^{\alpha}\, e_{(II)}^2\, t_{1(I)}^2 2t_{1(II)}^2\, e_{(I)}^{\beta}$, $a_1^2\, e_{(II)}^{\alpha}\, t_{1(I)}^2\, t_{1(II)}^2\, e_{(I)}^2\, t_{2(III)}^{\beta}$, $a_1^{\alpha}\, t_{1(I)}^2\, t_{1(II)}^2\, e_{(II)}^{\beta}$), and their conjugate configurations in M_4^{2+}, M_4, and M_4^{4+} analogues, respectively. Note the α, β and 2 superscripts in the electronic configuration indicate the electron with different spin orientations and pair-electron. Additionally, subscripts (I, II and III) denote the first, second and third orbitals in same symmetry. According to the highest contributing electronic configurations, the excitation from the $E_{(I)}$ ground to the A_1 excited state requires an electron to transfer from the a_1 HOMO to the $e_{(I)}$ lowest unoccupied molecular orbital (LUMO) of the respective states. This shows a $a_1 \rightarrow e_{(I)}$ electron excitation in M_4^{2+} analogues.

3.4 *PJTE problem methodology*

To figure out the details of the $(E_{(I)} + A_1 + E_{(II)}) \otimes e$ PJTE problem, the wave functions of two E degenerate ground states, $E_{(I)}$ and $E_{(II)}$, and an A_1 excited state were proposed as $|E_{(I)}\rangle$, $|E_{(II)}\rangle$, and $|A_1\rangle$ with the energy gap between the ground states and contributing excited states are indicated by Δ. First and second mathematical derivatives of *H* (electronic Hamiltonian) with respect to instability direction of *Q* were applied to specify the relations between $K_{0_{(1)}}$, $K_{0_{(2)}}$ and $K_{0_{(3)}}$ primary force constants in equation (1).

$$\begin{aligned} K_{0_{(1)}} &= \langle E_{(I)}|\partial^2 H/\partial Q^2|E_{(I)}\rangle, \\ K_{0_{(2)}} &= \langle E_{(II)}|\partial^2 H/\partial Q^2|E_{(II)}\rangle, \\ K_{0_{(3)}} &= \langle A_1|\partial^2 H/\partial Q^2|A_1\rangle. \end{aligned} \tag{1}$$

$F_{E_{(I)}A_1}$ and $G_{E_{(II)}A_1}$ are the vibronic coupling constants which, for simplicity, are called *F* and *G* here, as given by equation (2):

$$\begin{aligned} F_{E_{(I)}A_1} &= \langle E_{(I)}|\partial H/\partial Q|A_1\rangle, \\ G_{E_{(II)}A_1} &= \langle E_{(II)}|\partial H/\partial Q|A_1\rangle. \end{aligned} \tag{2}$$

Based on the PJTE theorem [13,16], the secular matrix equation of the perturbation theory for the three-level $(E_{(I)} + A_1 + E_{(II)}) \otimes e$ PJTE problem can be formulated as follows ($K_{0_{(1)}}$, $K_{0_{(2)}}$, $K_{0_{(3)}}$ primary force constants are denoted by K_1, K_2, K_3):

$$\begin{vmatrix} \frac{K_1}{2}Q^2 - \varepsilon & 0 & FQ \\ 0 & \frac{K_2}{2}Q^2 - \varepsilon & GQ \\ FQ & GQ & \frac{K_3}{3}Q^2 + \Delta - \varepsilon \end{vmatrix} = \begin{vmatrix} a - \varepsilon & 0 & f \\ 0 & b - \varepsilon & g \\ f & g & c - \varepsilon \end{vmatrix} = 0, \tag{3}$$

while *a*, *b*, *c*, *f* and *g* constants are denotations and the equation can be re-arranged as equation (4).

$$\varepsilon^3 - (a+b+c)\varepsilon^2 + \left(ab + ac + bc - f^2 - g^2\right)\varepsilon - abc + cf^2 + bg^2 = 0. \tag{4}$$

Table 2. Main electronic configurations and their weight coefficients in $M_4^{(2+,\ 0,4+)}$ (M = P, As, Sb) analogues (α and β denote electron in different orientations and I, II and III subscripts indicate the first, second and third orbitals in same symmetry, respectively).

State symmetry	Electronic configuration	Weight coefficients			Electronic configuration	Weight coefficients		
		P_4^{2+}	As_4^{2+}	Sb_4^{2+}		P_4	As_4	Sb_4
$E_{(II)}$	$a_1^2\ e_{(II)}^2\ t_{1(I)}^2\ t_{1(II)}^2$	−0.650	−0.638	−0.631	$a_1^2\ e_{(II)}^2\ t_{1(I)}^2\ t_{1(II)}^2\ e_{(I)}^2$	0.941	0.925	0.918
	$a_1^2\ e_{(I)}^2\ t_{1(I)}^2\ t_{1(II)}^2$	0.650	0.638	0.631	$a_1^2\ e_{(II)}^2\ t_{1(I)}^2\ t_{1(II)}^2\ e_{(I)}^{\alpha}\ t_{1(III)}^{\beta}$	0.000	0.014	0.017
	$e_{(II)}^2\ e_{(I)}^2\ t_{1(I)}^2\ t_{1(II)}^2$	−0.198	−0.207	−0.220	$a_1^2\ e_{(II)}^2\ t_{1(I)}^2\ t_{1(II)}^2\ e_{(I)}^{\beta}\ t_{1(III)}^{\alpha}$	−0.000	−0.014	−0.017
	$a_1^2\ e_{(II)}^2\ t_{1(I)}^2\ e_{(I)}^2$	0.099	0.103	0.110	$a_1^2\ e_{(II)}^2\ t_{1(I)}^2\ e_{(I)}^2\ t_{2(I)}^{\alpha}\ t_{2(II)}^{\beta}$	0.004	0.014	0.000
	$a_1^2\ e_{(II)}^2\ t_{1(II)}^2\ e_{(I)}^2$	0.099	0.103	0.110	$a_1^2\ e_{(II)}^2\ t_{1(I)}^2\ e_{(I)}^2\ t_{2(I)}^{\beta}\ t_{2(II)}^{\alpha}$	−0.004	−0.014	−0.001
$E_{(I)}$	$a_1^2\ e_{(II)}^2\ t_{1(I)}^2\ t_{1(II)}^2$	−0.650	−0.638	−0.631	$a_1^2\ e_{(II)}^2\ t_{1(I)}^2\ t_{1(II)}^2\ e_{(I)}^2$	−0.004	0.001	−0.005
	$a_1^2\ e_{(I)}^2\ t_{1(I)}^2\ t_{1(II)}^2$	0.650	0.638	0.631	$a_1^2\ e_{(II)}^2\ t_{1(I)}^2\ t_{1(II)}^2\ e_{(I)}^{\alpha}\ 3t_1^{\beta}$	0.577	0.572	0.575
	$e_{(II)}^2\ e_{(I)}^2\ t_{1(I)}^2\ t_{1(II)}^2$	−0.212	−0.210	−0.216	$a_1^2\ e_{(II)}^2\ t_{1(I)}^2\ t_{1(II)}^2\ e_{(I)}^{\beta}\ 3t_1^{\alpha}$	−0.577	−0.572	−0.575
	$a_1^2\ e_{(II)}^2\ t_{1(I)}^2\ e_{(I)}^2$	−0.212	−0.210	−0.216	$a_1^2\ e_{(II)}^2\ t_{1(I)}^2\ e_{(I)}^2\ t_{2(I)}^{\alpha}\ t_{2(II)}^{\beta}$	0.208	0.198	0.207
	$a_1^2\ e_{(II)}^2\ t_{1(II)}^2\ e_{(I)}^2$	−0.212	−0.210	−0.216	$a_1^2\ e_{(II)}^2\ t_{1(I)}^2\ e_{(I)}^2\ t_{2(I)}^{\beta}\ t_{2(II)}^{\alpha}$	−0.208	−0.198	−0.207
A_1	$a_1^{\alpha}\ e_{(II)}^2\ t_{1(I)}^2\ t_{1(II)}^2\ e_{(I)}^{\beta}$	0.623	0.612	0.605	$a_1^2\ e_{(II)}^{\alpha}\ t_{1(I)}^2\ t_{1(II)}^2\ e_{(I)}^2\ 3t_2^{\beta}$	−0.646	−0.620	−0.621
	$a_1^{\beta}\ e_{(II)}^2\ t_{1(I)}^2\ t_{1(II)}^2\ e_{(I)}^{\alpha}$	−0.623	−0.612	−0.605	$a_1^2\ e_{(II)}^{\beta}\ t_{1(I)}^2\ t_{1(II)}^2\ e_{(I)}^2\ 3t_2^{\alpha}$	0.646	0.620	0.621
	$a_1^{\alpha}\ e_{(II)}^{\beta}\ t_{1(I)}^2\ t_{1(II)}^2\ e_{(I)}^2$	0.000	0.000	0.000	$a_1^2\ e_{(II)}^2\ 2a_1^{\alpha}\ t_{1(I)}^2\ t_{1(II)}^2\ e_{(I)}^{\beta}$	0.148	0.193	0.172
	$a_1^{\beta}\ e_{(II)}^{\alpha}\ t_{1(I)}^2\ t_{1(II)}^2\ e_{(I)}^2$	0.000	0.000	0.000	$a_1^2\ e_{(II)}^2\ 2a_1^{\beta}\ t_{1(I)}^2\ t_{1(II)}^2\ e_{(I)}^{\alpha}$	−0.148	−0.193	−0.172
$T_1(I)$	$a_1^2\ e_{(II)}^{\alpha}\ t_{1(I)}^{\beta}\ t_{1(II)}^2\ e_{(I)}^2$	0.577	0.566	0.563	$a_1^2\ e_{(II)}^2\ t_{1(I)}^2\ t_{1(II)}^2\ e_{(I)}^{\alpha}\ t_{2(II)}^{\beta}$	0.572	0.561	0.497
	$a_1^2\ e_{(II)}^{\beta}\ t_{1(I)}^{\alpha}\ t_{1(II)}^2\ e_{(I)}^2$	−0.577	−0.566	−0.563	$a_1^2\ e_{(II)}^2\ t_{1(I)}^2\ t_{1(II)}^2\ e_{(I)}^{\beta}\ t_{2(II)}^{\alpha}$	−0.572	−0.561	−0.497
	$a_1^2\ e_{(II)}^2\ t_{1(I)}^2\ t_{1(II)}^{\alpha}\ e_{(I)}^{\beta}$	−0.333	−0.327	−0.325	$a_1^2\ e_{(II)}^{\alpha}\ t_{1(I)}^2\ t_{1(II)}^2\ e_{(I)}^2\ t_{2(I)}^{\beta}$	0.318	0.303	0.402
	$a_1^2\ e_{(II)}^2\ t_{1(I)}^2\ t_{1(II)}^{\beta}\ e_{(I)}^{\alpha}$	0.333	0.327	0.325	$a_1^2\ e_{(II)}^{\beta}\ t_{1(I)}^2\ t_{1(II)}^2\ e_{(I)}^2\ t_{2(I)}^{\alpha}$	−0.318	−0.303	−0.402
$T_1(II)$	$a_1^2\ e_{(II)}^{\alpha}\ t_{1(I)}^2\ t_{1(II)}^{\beta}\ e_{(I)}^2$	0.577	0.566	0.563	$a_1^2\ e_{(II)}^2\ t_{1(I)}^2\ t_{1(II)}^2\ e_{(I)}^{\alpha}\ t_{2(I)}^{\beta}$	0.554	0.502	0.552
	$a_1^2\ e_{(II)}^{\beta}\ t_{1(I)}^2\ t_{1(II)}^{\alpha}\ e_{(I)}^2$	−0.577	−0.566	−0.563	$a_1^2\ e_{(II)}^2\ t_{1(I)}^2\ t_{1(II)}^2\ e_{(I)}^{\beta}\ t_{2(I)}^{\alpha}$	−0.554	−0.502	−0.552
	$a_1^2\ e_{(II)}^2\ t_{1(I)}^{\alpha}\ t_{1(II)}^2\ e_{(I)}^{\beta}$	−0.333	−0.327	−0.325	$a_1^2\ e_{(II)}^{\alpha}\ t_{1(I)}^2\ t_{1(II)}^2\ e_{(I)}^2\ t_{2(II)}^{\beta}$	0.358	0.406	0.302
	$a_1^2\ e_{(II)}^2\ t_{1(I)}^{\beta}\ t_{1(II)}^2\ e_{(I)}^{\alpha}$	0.333	0.327	0.325	$a_1^2\ e_{(II)}^{\beta}\ t_{1(I)}^2\ t_{1(II)}^2\ e_{(I)}^2\ t_{2(II)}^{\alpha}$	−0.358	−0.406	−0.302
$T_1(III)$	$a_1^2\ e_{(II)}^{\alpha}\ t_{1(I)}^2\ e_{(I)}^2\ t_{1(III)}^{\beta}$	0.667	0.654	0.650	$a_1^2\ e_{(II)}^{\alpha}\ t_{1(I)}^2\ t_{1(II)}^2\ e_{(I)}^2\ t_{2(III)}^{\beta}$	0.156	0.205	0.184
	$a_1^2\ e_{(II)}^{\beta}\ t_{1(I)}^2\ e_{(I)}^2\ t_{1(III)}^{\alpha}$	−0.667	−0.654	−0.650	$a_1^2\ e_{(II)}^{\beta}\ t_{1(I)}^2\ t_{1(II)}^2\ e_{(I)}^2\ t_{2(III)}^{\alpha}$	−0.156	−0.205	−0.184
	$a_1^2\ e_{(II)}^{\alpha}\ t_{1(I)}^2\ e_{(I)}^2\ t_{1(III)}^{\beta}$	−0.172	−0.179	−0.191	$a_1^2\ e_{(II)}^2\ 2a_1^{\alpha}\ t_{1(I)}^2\ t_{1(II)}^2\ e_{(I)}^{\beta}$	0.626	0.605	0.597
	$a_1^2\ e_{(II)}^{\beta}\ t_{1(I)}^2\ e_{(I)}^2\ t_{1(III)}^{\alpha}$	0.172	0.179	0.191	$a_1^2\ e_{(II)}^2\ 2a_1^{\beta}\ t_{1(I)}^2\ t_{1(II)}^2\ e_{(I)}^{\alpha}$	−0.626	−0.605	−0.597

State symmetry	Electronic configuration	Weight coefficients		
		P_4^{4+}	As_4^{4+}	Sb_4^{4+}
$E_{(II)}$	$a_1^2\ t_{1(I)}^2\ t_{1(II)}^2$	0.831	0.836	0.825
	$a_1^2\ e_{(II)}^2\ t_{1(I)}^2$	−0.217	−0.115	−0.109
	$e_{(II)}^2\ t_{1(I)}^2\ t_{1(II)}^2$	−0.132	−0.201	−0.174
	$a_1^2\ e_{(II)}^2\ e_{(I)}^2$	0.147	0.100	0.109
	$a_1^2\ t_{1(I)}^2\ e_{(I)}^2$	−0.144	−0.196	−0.180
$E_{(I)}$	$a_1^2\ t_{1(I)}^2\ t_{1(II)}^2$	0.244	0.052	0.019
	$a_1^2\ e_{(II)}^2\ t_{1(I)}^2$	0.527	0.643	0.387
	$e_{(II)}^2\ t_{1(I)}^2\ t_{1(II)}^2$	−0.288	−0.254	−0.295
	$a_1^2\ e_{(II)}^2\ e_{(I)}^2$	−0.186	−0.206	−0.244
	$a_1^2\ t_{1(I)}^2\ e_{(I)}^2$	0.209	0.114	0.139

Table 2. continued

State symmetry	Electronic configuration	Weight coefficients		
		P_4^{4+}	As_4^{4+}	Sb_4^{4+}
A_1	$a_1^{\alpha}\, t_{1(II)}^{\ 2}\, e_{(II)}^{\ \beta}$	0.512	0.612	0.612
	$a_1^{\beta}\, t_{1(II)}^{\ 2}\, e_{(II)}^{\ \alpha}$	−0.512	−0.612	−0.612
	$a_1^{\ 2}\, t_{1(I)}^{\ \alpha}\, t_{1(II)}^{\ \beta}\, e_{(II)}^{\ 2}$	−0.215	−0.123	0.132
	$a_1^{\ 2}\, t_{1(I)}^{\ \beta}\, t_{1(II)}^{\ \alpha}\, e_{(II)}^{\ 2}$	0.215	0.123	−0.132
T_1(I)	$a_1^{\ 2}\, e_{(II)}^{\ \alpha}\, t_{1(I)}^{\ 2}\, t_{1(II)}^{\ \beta}$	−0.360	−0.595	−0.617
	$a_1^{\ 2}\, e_{(II)}^{\ \beta}\, t_{1(I)}^{\ 2}\, t_{1(II)}^{\ \alpha}$	0.360	0.595	0.617
	$a_1^{\ 2}\, t_{1(I)}^{\ 2}\, t_{1(II)}^{\ \alpha}\, e_{(I)}^{\ \beta}$	0.555	−0.295	−0.229
	$a_1^{\ 2}\, t_{1(I)}^{\ 2}\, t_{1(II)}^{\ \beta}\, e_{(I)}^{\ \alpha}$	−0.555	0.295	−0.229
T_1(II)	$a_1^{\ 2}\, e_{(II)}^{\ \alpha}\, t_{1(I)}^{\ 2}\, t_{1(II)}^{\ \beta}$	−0.637	−0.605	−0.571
	$a_1^{\ 2}\, e_{(II)}^{\ \beta}\, t_{1(I)}^{\ 2}\, t_{1(II)}^{\ \alpha}$	0.637	0.605	0.571
	$a_1^{\ 2}\, t_{1(I)}^{\ \alpha}\, t_{1(II)}^{\ 2}\, e_{(I)}^{\ \beta}$	0.179	0.268	0.346
	$a_1^{\ 2}\, t_{1(I)}^{\ \beta}\, t_{1(II)}^{\ 2}\, e_{(I)}^{\ \alpha}$	−0.179	−0.268	−0.346
T_1(III)	$a_1^{\ 2}\, t_{1(I)}^{\ \alpha}\, t_{1(II)}^{\ \beta}\, e_{(I)}^{\ 2}$	−0.193	−0.166	−0.183
	$a_1^{\ 2}\, t_{1(I)}^{\ \beta}\, t_{1(II)}^{\ \alpha}\, e_{(I)}^{\ 2}$	0.193	0.166	0.183
	$a_1^{\alpha}\, t_{1(I)}^{\ 2}\, t_{1(II)}^{\ 2}\, e_{(I)}^{\ \beta}$	−0.284	−0.139	−0.129
	$a_1^{\beta}\, t_{1(I)}^{\ 2}\, t_{1(II)}^{\ 2}\, e_{(I)}^{\ \alpha}$	0.284	0.139	0.129

* Note that $2a_1$ denotes the second orbital with a_1 symmetry.

Table 3. PJTE coupling constants, F and G ($eV\text{Å}^{-1}$), energy gap Δ (eV), primary force constants, K_1, K_2 and K_3 ($eV\text{Å}^{-2}$) of M_4^{2+} (M = P, As, Sb) analogues through fitting equation (5) to calculate the APES cross-sections in figure 2.

Analogues	K_1	K_2	K_3	F	G	Δ
P_4^{2+}	1.07	1.56	1.14	1.39	2.28	0.23
As_4^{2+}	0.59	1.30	0.92	1.02	1.61	0.13
Sb_4^{2+}	0.35	1.17	0.90	0.87	1.33	0.09

The relations between roots of the 3 × 3 secular equation (ε_1, ε_2 and ε_3) are given in equation (5):

$$\begin{cases} \varepsilon_1 + \varepsilon_2 + \varepsilon_3 = a + b + c, \\ \varepsilon_1\varepsilon_2 + \varepsilon_2\varepsilon_3 + \varepsilon_1\varepsilon_3 = ab + ac + bc - f^2 - g^2, \\ \varepsilon_1\varepsilon_2\varepsilon_3 = abc + cf^2 + bg^2. \end{cases} \tag{5}$$

In equation (4), we face a system of three equations with five unknowns to solve. To estimate the values of K_1, K_2, K_3, F and G, the solution to equation (5) is required. Solutions for small Q values should coincide with the *ab initio* calculated energy profiles in the Q_e direction. Subsequently, the PJTE coupling constants (F and G), and the primary force constants (K_1, K_2, K_3) were estimated by fitting the energies to obtain the APES cross-sections in figure 2 and displayed in table 3.

The occurrence of the PJTE in M_4^{4+} (M = P, As, Sb) analogues affected the stability of the ground state making the $E_{(I)}$ unstable ($E_{(II)}$ is still stable in all M_4^{2+} analogues). The necessary condition for instability in the $E_{(I)}$ ground sate around the Q_e normal coordinate is when $K_1 - (G^2/\Delta) < 0$ [16].

Meanwhile, K_1 characterizes the stiffness of the system with respect to the distortion, as well as instability for the $E_{(I)}$ ground state, in the series. Table 3 illuminates that the above condition occurs for all M_4^{2+} (M = P, As, Sb) analogues with P_4^{2+} distorting more than As^{2+}, Sb^{2+} analogues due to the pseudo Jahn–Teller interactions.

3.5 *Stability in $M_4^{(0,+4)}$ tetrahedral structures*

As revealed by adding and removing a pair of electrons from the M_4^{2+}, to simulate the $M_4^{(0,+4)}$ analogues, a similarity in the situation of the applied active spaces has been predicted for the $M_4^{(2+,0,+4)}$ analogues. However, geometrical and frequency calculations for the M_4 and M_4^{4+} analogues do not show an imaginary frequency in the aforementioned series. Hence, the $M_4^{(0,+4)}$ holds a high T_d symmetry structure and are stable in their pyramidal tetrahedral structure.

To rationalize the reason of stability TH in $M_4^{(0,+4)}$ analogues, we need to compare the electronic configurations specifically in the $E_{(I)}$ ground and A_1 excited states. From

table 2, it was demonstrated that (a_1^2 $e_{(II)}^2$ $t_{1(I)}^2$ $t_{1(II)}^2$ and a_1^2 $e_{(II)}^2$ $t_{1(I)}^2$ $t_{1(II)}^2$ $e_{(I)}^2$) are the main electronic configuration for the M_4^{+2} and M_4 analogues. Indeed, a pair of electrons are added to the $e_{(I)}^2$ orbital in the M_4. Due to the $a_1 \rightarrow e_{(I)}$ electron excitation, the M_4 analogues' $e_{(I)}{}^2$ orbital is particularly occupied and the $(E_{(I)} + A_1 + E_{(II)}) \otimes e$ PJTE problem, which is the reason of instability, cannot occur in the M_4 analogues. Additionally, $a_1{}^2$ $t_{1(I)}{}^2$ $t_{1(II)}{}^2$, and $a_1{}^{\alpha}$ $t_{1(I)}{}^2$ $t_{1(II)}{}^2$ $e_{(I)}{}^{\beta}$ being the main electronic configurations for the $E_{(I)}$ ground and A_1 excited states in the M_4^{+4} displays that an electron from the HOMO, a_1, excites to the LUMO, $e_{(II)}$, which is not an appropriate excitation for the $(E_{(I)} + A_1) \otimes e$ PJTE problem. However, as the $E_{(II)}$ ground state in the M_4^{2+} is stable, the $a_1 \rightarrow e_{(II)}$ excitation does not affect the TH structure in the M_4^{+4} analogues. In summary, by adding or removing a pair of electrons to the M_4^{+4} analogues, the $a_1 \rightarrow e_{(I)}$ electron excitation is maladjusted and the PJTE is suppressed in the series. Therefore, TH structure in $M_4^{(0,+4)}$ analogues are stable.

4. Conclusions

The origin of symmetry descent in the M_4^{2+} (M = P, As, Sb) analogues due to pseudo Jahn–Teller interactions is explored and the secular matrix equation of the $(E_{(I)} + A_1 + E_{(II)}) \otimes e$ problem, which is the reason of TH configuration instability for considered series, was formulated according to the perturbation theory. The corresponding vibronic coupling constants were estimated by fitting the energies to obtain the APES cross-sections. To rationalize how the occurrence PJTE in the M_4^{2+} analogues can be suppressed, the electronic configuration for the $M_4^{(2+,\ 0,\ +4)}$ analogues were analysed and the electron excitation belongs to the $M_4^{(0,\ +4)}$ analogues, which are stable in their TH structure, were compared with the M_4^{+2} analogues.

Acknowledgements

The corresponding author wishes to appreciate the Yazd Branch, Islamic Azad University, for their financial support of this research. All calculations were enabled in part with support from Westgrid (www.westgrid.ca) and Compute/Calcul Canada (www.computecanada.ca).

References

[1] Kutzelnigg W 1984 *Angew. Chem. Int. Ed.* **23** 272
[2] Ahlrichs R, Brode S and Ehrhardt C 1985 *J. Am. Chem. Soc.* **107** 7260
[3] Bock H and Muller H 1984 *Inorg. Chem.* **23** 4365
[4] Schmidt M W and Gordon M S 1985 *Inorg. Chem.* **24** 4503
[5] Karton A and Martin J M 2007 *Mol. Phys.* **105** 2499
[6] Wang L P, Tofan D, Chen J, Van Voorhis T and Cummins C C 2013 *RSC Adv.* **3** 23166
[7] Oakley M S, Bao J, Klobukowski M, Truhlar D G and Gagliardi L 2018 *J. Phys. Chem. A* **122** 5742
[8] Corbridge D E C 1974 *Structural chemistry of phosphorus* (The Netherlands: Elsevier Scientific Publishing Company)
[9] Wang L S, Niu B, Lee Y T, Shirley D A, Ghelichkhani E and Grant E R 1990 *J. Chem. Phys.* **93** 6318
[10] Wang L S, Niu B, Lee Y T, Shirley D A, Ghelichkhani E and Grant E R 1990 *J. Chem. Phys.* **93** 6327
[11] Meiswinkel R and Koppel H 1993 *Chem. Phys. Lett.* **201** 449
[12] Englman R 1972 *The Jahn–Teller effect in molecules and crystals* (New York: Wiley Interscience)
[13] Bersuker I B 2006 *The Jahn–Teller effect* (Cambridge: Cambridge University Press)
[14] Applegate B E, Barckholtz T A and Miller T A 2003 *Chem. Soc. Rev.* **32** 38
[15] Bhattacharyya S, Opalka D and Domcke W 2015 *Chem. Phys.* **460** 51
[16] Bersuker I B 2013*Chem. Rev.* **113** 1351
[17] Liu Y, Bersuker I B and Boggs J E 2013 *Chem. Phys.* **417** 26
[18] Liu Y, Bersuker I B, Garcia-Fernandez P and Boggs J E 2012 *J. Phys. Chem. A* **116** 7564
[19] Ilkhani A R and Monajjemi M 2015 *Comput. Theor. Chem.* **1074** 19
[20] Ilkhani A R 2017 *Quim. Nova* **40** 491
[21] Hermoso W, Ilkhani A R and Bersuker I B 2014 *Comput. Theor. Chem.* **1049** 109
[22] Ilkhani A R, Hermoso W and Bersuker I B 2015 *Chem. Phys.* **460** 75
[23] Ilkhani A R 2015 *J. Theor. Comput. Chem.* **6** 1550045
[24] Gorinchoy N N, Arsene I and Bersuker I B 2018 *J. Phys. Conf. Ser.* **1148** 012005
[25] Ilkhani A R 2017 *Russ. J. Phys. Chem. A* **91** 1743
[26] Ilkhani A R 2019 *J. Mol. Model.* **25** 8
[27] Ilkhani A R 2019 *Struct. Chem.* **30** 303
[28] Ilkhani A R 2019 *Chem. Pap.* **73** 85
[29] Ilkhani A R 2019 *J. Chem. Sci.* **131** 37
[30] Bhattacharyya K, Surendran A, Chowdhury C and Datta A 2016 *Phys. Chem. Chem. Phys.* **18** 31160
[31] Jose D and Datta A 2011 *Phys. Chem. Chem. Phys.* **13** 7304
[32] Ilkhani A R, Gorinchoy N N and Bersuker I B 2015 *Chem. Phys.* **460** 106
[33] Chowdhury C, Jahiruddin S and Datta A 2016 *J. Phys. Chem. Lett.* **7** 1288
[34] Pratik S Md, Chowdhury C, Bhattacharjee R, Jahiruddin Sk and Datta A 2015 *Chem. Phys.* **460** 101
[35] Ivanov A S, Miller E, Boldyrev A I, Kameoka Y, Sato T and Tanaka K 2015 *J. Phys. Chem. C* **119** 12008
[36] Ilkhani A R 2015 *J. Mol. Struct.* **1098** 21
[37] Jose D and Datta A 2012 *J. Phys. Chem. C* **116** 24639
[38] Ivanov A S, Bozhenko K V and Boldyrev A I 2012 *Inorg. Chem.* **51** 8868
[39] Sergeeva A P and Boldyrev A I 2010 *Organometallics* **29** 3951
[40] Pratik S Md and Datta A 2015 *J. Phys. Chem. C* **119** 15770
[41] Hu Y, Chen Z, Zhang H, Li M, Hou Z, Luo X *et al* 2017 *Drug Deliv.* **24** 1295
[42] Polly R, Werner H J, Manby F R and Knowles P J 2004 *Mol. Phys.* **102** 2311
[43] Werner H J and Meyer W 1981 *J. Chem. Phys.* **74** 5794

[44] Werner H J and Meyer W 1980 *J. Chem. Phys.* **73** 2342
[45] Werner H J and Knowles P J 1985 *J. Chem. Phys.* **82** 5053
[46] Wilson A K, Woon D E, Peterson K A and Dunning T H 1999 *J. Chem. Phys.* **110** 7667
[47] Woon D E and Dunning T H 1993 *J. Chem. Phys.* **98** 1358
[48] Dunning T H 1989 *J. Chem. Phys.* **90** 1007
[49] Dolg M 1996 *J. Chem. Phys.* **104** 4061
[50] Dolg M 1996 *Chem. Phys. Lett.* **250** 75
[51] Peterson K A 2003 *J. Chem. Phys.* **119** 11099
[52] Werner H J, Knowles P J, Manby F R and Schutz M 2015 MOLPRO, version 2015.1.22, a package of ab initio programs. Available: https://www.molpro.net (accessed on January 2015)